Inhibition effect of different interstitial materials on thermal runaway propagation in the cylindrical lithium-ion battery module

Inhibition effect of different interstitial materials on thermal runaway propagation in the cylindrical lithium-ion battery module

ChengchaoYuan[a,b], QingsongWang[c], Yu Wang[d], Yang Zhao[a,b*]

[a] *Department of Precision Machinery and Precision Instrumentation, University of Science and Technology of China, Hefei, Anhui 230027, PR China*

[b] *CAS Key Laboratory of Mechanical Behavior and Design of Materials, University of Science and Technology of China, Hefei, Anhui 230027, PR China*

[c]*State Key Laboratory of Fire Science, University of Science and Technology of China, Hefei 230026, PR China*

[d]*School of Engineering, BRE Centre for Fire Safety Engineering, University of Edinburgh, Edinburgh EH9 3JL, United Kingdom*

Nomenclature

A	surface area [m^2]
C_{can}	average mass specific heat of the can and cell material residual [J kg^{-1} K^{-1}]
C_{cell}	average mass specific heat of the vented cell materials [J kg^{-1} K^{-1}]
C_{total}	average mass specific heat of single cell [J kg^{-1} K^{-1}]
h_{conv}	convective heat transfer coefficient [W m^{-2} K^{-1}]
k	effective thermal conductivity [W m^{-1} K^{-1}]
m_{cell}	mass of an 18650 cell's components [kg]
m_{can}	mass of an 18650 cell's stainless-steel casing [kg]
m_{total}	mass of an 18650 cell [kg]
$\dot{Q}_{conv}$	convective heat transfer at the cell boundaries [W m^{-2}]
$\dot{Q}_{rad}$	radiative heat transfer at the cell boundaries [W m^{-2}]
$\dot{Q}_r$	chemical reaction heat generation rate [W]
$\dot{Q}_f$	solid electrolyte interface (SEI) decomposition heat generation rate [W]

$\dot{Q}_n$	Negative-Solvent reaction heat generation rate [W]
$\dot{Q}_p$	Positive-Solvent reaction heat generation rate [W]
$\dot{Q}_e$	electrolyte decomposition heat generation rate [W]
t	time [s]
T	temperature [K]
T_0	initial exothermic temperature [K]
dT/dt	the derivative of the temperature [K s^{-1}]
Greek symbols	
ε	Emissivity of the battery surface
σ	Stefan-Boltzmann constant, 5.67e-8 [W m^{-2} K^{-4}]
TR_T	TR triggering temperature

HIGHLIGHTS

Inhibition effect of interstitial materials on TR in battery modules is studied.

CFD model is used to analyze battery temperature under different conditions.

The simulation is experimentally compared and verified by basic safety units.

Composite graphite sheet and Al extrusion can effectively control the thermal path.

ABSTRACT

With the growing demand for high specific energy density of lithium-ion battery pack in electric vehicle to relieve range anxiety, thermal stability in abused conditions is becoming increasingly important in battery pack safety design. Most of the fire accidents are resulted from the thermal runaway (TR) of a single cell and then propagate to the battery modules and entire pack. This study focuses on the safety enhancement methods for battery module, which is filled with different interstitial materials. The basic safety unit is composed of 11 commercial 18650 cylindrical cells, which is isolated from the electric vehicle pack as the test module. The test modules were intentionally triggered into TR by heating wire to evaluate the TR propagation

resistance. A model based on finite volume method was established to simulate the TR propagation. The results of both simulation and experiments show that the protection of neighboring cells from different interstitial materials varies significantly. Graphite composite sheet and Al extrusion as interstitial materials could effectively suppress TR propagation. The results also indicate that for safety design of battery pack, thermal path should be effectively controlled, and particularly the combustion of expelled electrolyte must be directed away from adjacent cells.

Key words: Electric vehicle; Lithium-ion battery safety; Thermal runaway; Interstitial material; Thermal runaway propagation

1. Introduction

Lithium-ion (Li-ion) batteries, as the state-of-the-art energy storage units, have been mainly applied in the fields of Energy Storage System (ESS) [1], such as Electric Vehicle (EV) [2], auxiliary power unit (APU), smart grids, etc. The industry of EV has boomed worldwide since 2009 due to the concerns of dependence on oil-based fuels consumption and the pressure of carbon emissions. Battery electric vehicles access the mass market rapidly with their advantages of zero emission and also the generous subsidies from governments. Rechargeable li-ion batteries have been widely used in consumer electronic devices, such as cell phones and computers [3-6]. Due to its high gravimetric and volumetric energy densities [7], Li-ion battery is currently the best power source candidate for BEV compared to NiMH or lead-acid battery. However, higher energy density may cause greater thermal hazard if this energy is released abruptly because of contamination, manufacturing defect, mechanical insult, overcharging or internal short circuit caused by overheating [8-10], etc. The rapid discharge of electrical energy inside the cell will raise its temperature and causes series reactions, including 1) reaction between cathode and electrolyte; 2) thermal decomposition of electrolyte; 3) reaction between electrolyte and anode; 4) thermal

decomposition of anode; 5) thermal decomposition of cathode [11-13]. This auto-acceleratory exothermic process is called thermal runaway (TR), which generates combustible gases, and results in expulsions of the cell components [14-16]. Generally, there are three ways to improve the safety performance of lithium-ion battery to prevent TR: 1) enhance thermal stability of the electrode materials; 2) improve the electrolyte of lithium-ion battery to avoid burning; 3) propose new design and management of lithium-ion battery through some external methods, such as safety design and insulation of cells, safety valves and the process improvement [17-19].

The safety issues of Li-ion batteries have drawn tremendous attention and become an urgent problem to be solved in the development of Li-ion batteries. Some typical battery pack safety accidents are shown in Table 1. However, the risk of thermal runaway becomes even more severe in large scale battery pack since failure of a single cell could trigger a TR propagation in the whole pack, which may cause catastrophic damages.

Table 1

Typical accidents related to Li-ion batteries

Date/Place	Brand	Power type	Cause
May 2011/USA	Chevrolet Volt	BEV	Caught fire after crash test
2012/Texas	Fisker Karma	HEV	Unknown
Jan 7 2013/Boston's Logan International Airport	Boeing 787 Dreamliner	APU	Internal short circuit
Jan 1 2016/ Norway Gjerstad	Tesla MODEL S	BEV	Distribution box short circuit
Apr 9 2016/Shanghai	BYD	HEV	Foreign body in exhaust pipe
May 14 2016/Zhuhai	Yinlong	BEV	Battery short circuit
June 23 2016/Beijing	JAC iEV5	BEV	Unknown

For a battery pack that is in working status, there are several factors that may lead to thermal runaway, such as mechanical abuse (puncture, crush), electrical abuse (overcharge, over-discharge, short circuit), thermal abuse, etc [20, 21]. Generally,

Battery Management System (BMS) and Battery Thermal Management System (BTMS) [22, 23] can monitor and control the real-time safety related parameters (temperature, voltage, current, pressure, etc.) to prevent the batteries from being abused. However, the manufacturing defects (loose connection, separator damage, foreign debris) inside the batteries cannot be monitored or controlled by BMS and BTMS, which may still cause thermal runaway of batteries. Passive inhibition methods are required to limit the TR propagation, and thus avoid catastrophic break down of the whole system.

Currently, some experimental and simulation works about safety are based on cell level. Saw et al. have improved the safety performance of single cell by studying the surface roughness and coating thickness of boron nitride added on battery casing [24]. Coman et al. [25] have studied different processes of cylindrical cell during TR in a model with venting and quantified the mass fraction of electrolyte leaving the cell can. In addition, there are a few researches aiming at enhancing the safety of battery module. Guo et al. [26] have developed three-dimensional thermal abuse model on the high capacity lithium-ion batteries, which contributes to the design of cooling system in the battery packs. In the normal working status, a 3D thermal model of lithium-ion battery pack is developed to simulate the thermal behaviors of the EV power battery [27]. What's more, there are some novel thermal studies about battery module: aluminum foam with porosity control used as cooling system [28], influence of discharging treatment and module shape on the thermal failure propagation [29], and the impact of electrical connections on 18650 cell TR propagation and failure behaviors of pouch cells [30], etc. Abada et al. [31] summarized the phenomenon, mechanism and safety approach of thermal runaway in both cell level and module level.

For different kinds of ESS, a price and weight competitive safety grouping scheme is needed to improve the TR resistance of the lithium battery module. Therefore, we proposed four interstitial materials (air, Al plate, graphite composite sheet and Al extrusion) with different potential application values, and studied their inhibition effects on TR propagation. The system studied in this paper is a simplified form of a certain module in the battery pack, which contains 11 parallel cells with various TR propagation paths once TR occurs, and we call it Basic Safety Unit (BSU). Different

interstitial materials are inserted between cells to investigate their effects on thermal inhibition, and the middle cell of the module was heated into TR in the mode of top venting or side rupture. The TR propagation results were studied in both simulation and experimental methods.

2. Development of Thermal Model

2.1 Thermal runaway mechanism

The understanding of the mechanism of TR in a lithium-ion cell is critical when designing the thermal management systems, which should mitigate the effects of TR and impede cell-to-cell propagation. TR means uncontrolled temperature rise of a single cell caused by the exothermic chain reactions and is characterized by a distinct rapid increase of temperature, rather than a steady temperature rise. Energy released during TR in a cell includes cell body energy, top venting energy and side rupture energy, as shown in Fig. 1. The heat released from an abused cell can activate chain reactions in the neighboring cells, causing catastrophic failure of the whole battery module or pack.

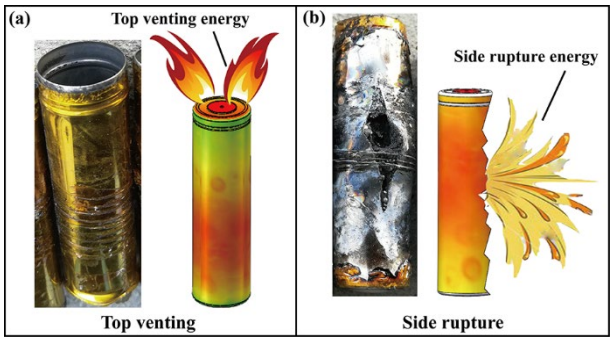

Fig. 1. Schematic of energy constitution (Physical and model drawing).

A TR propagation model was built to analyze the heat transfer through different paths. To simplify the analysis and to focus on the propagation process, some assumptions are proposed as follows [32-34]: the heat transfer condition of TR is set to be adiabatic; residual burning is not considered; the cell is considered as a thermally lumped system; vented gases are not considered as reactive and no combustion is taking place in between the cells. Structural integrity and material properties are assumed to

be constant at high temperatures. Every cell conforms to the energy balance equation, as illustrated in Fig. 2 [35]. The increase of the internal energy of each cell is determined by the heat generation inside the cell and the heat dissipation rate. The heat generation is induced by chemical reaction and Joule heating due to electrical short circuit. The heat dissipation includes conduction, convection and radiation.

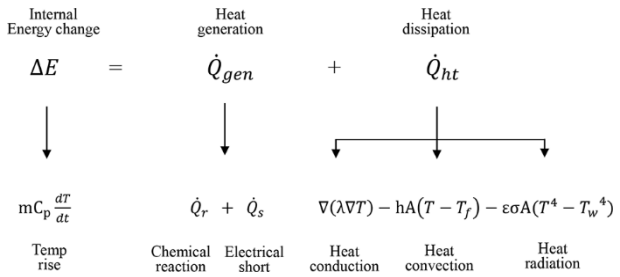

Fig. 2. Energy balance equation of a single cell.

In the normal working conditions, $\dot{Q}_s$ is the main source of the heat generation. When TR occurs in the system, the energy release rate due to chemical reaction $\dot{Q}_r$ is much larger than $\dot{Q}_s$ from Joule heating rate [32], thus only the effect of $\dot{Q}_r$ is taken into consideration. Generally, $\dot{Q}_r$ contains the following four parts:

$$\dot{Q}_r = \dot{Q}_f + \dot{Q}_n + \dot{Q}_p + \dot{Q}_e \quad (1)$$

Where $\dot{Q}_f$ is the heat generation rate due to the decomposition of SEI, $\dot{Q}_n$ due to Negative-Solvent reaction, $\dot{Q}_p$ due to Positive-Solvent reaction, and $\dot{Q}_e$ is the heat generation rate due to the decomposition of electrolyte.

The heat dissipates from the system to the surroundings through convection and radiation, and can be written as follows:

$$\dot{Q}_{conv} = h_{conv}A(T - T_f) \quad (2)$$

$$\dot{Q}_{rad} = \varepsilon\sigma A(T^4 - T_w^4) \quad (3)$$

Based on energy balance equations as shown in Eq. (1) - (3), the temperature distribution inside the system under a certain TR condition can be solved using numerical simulation tool - FLUENT. The results from the simulation can be used to predict the most possible location where TR occur and make it possible to prevent it from happening in advance.

158 *2.2 Calibration of thermal properties of single cells*

159 Accelerating rate calorimeter (EV-ARC, Thermal hazard technology, UK) was
160 used to measure the thermal hazard and runaway characteristics of commercial 18650
161 lithium-ion batteries, as shown in Fig. 3(a). The thermal runaway energy distribution
162 can be calibrated during the experiment [32, 35]. The change of the temperature during
163 TR is recorded in an adiabatic environment, as shown in Fig. 3(b) & (c).

164 A standard heat-wait-search (HWS) procedure is the most characteristic and
165 prevalent way to determine the onset temperature of self-heating. The tests evaluated
166 the thermal hazard characteristics, such as initial exothermic temperature (T_0) and self-
167 heating rate (dT/dt), as shown in Fig. 3 (d) & (e). The maximum self-heating power of
168 commercial 18650 cylindrical lithium-ion battery cells (Samsung 18650-33G) of 100%
169 state of charge (SOC) was measured to be 9.95 kW, and the maximum temperature
170 reached 889 ^{o}C.

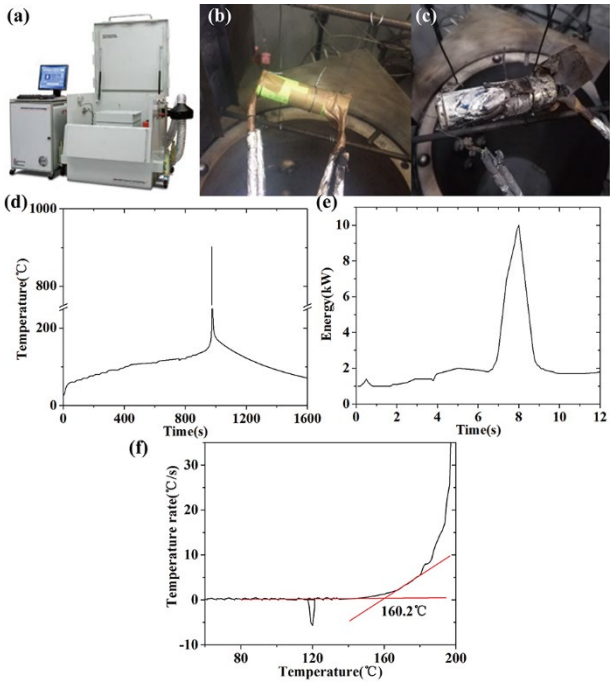

171

172 **Fig. 3.** Accelerating rate calorimeter (ARC) test process. (a)ARC test device; (b) & (c) Cell status
173 before & after ARC test; (d) Thermal runaway temperature of a cell; (e) energy release variation
174 curve of a cell; (f) Temperature rate as a function of temperature, T_0 was defined as the point at
175 which the heating-rate curve rises from constant to quasi-exponential.

176 After the experiment proceeded for 960 seconds, it was recorded that the rate of

the temperature rise of the cell increased rapidly. T_0 was defined as the point at which the heating-rate curve rises from constant to quasi-exponential [36], and was used as the TR triggering temperature (TR_T) to determine if the cell was forced into TR in simulation. T_0 was 160.6±1.2 ºC on average recorded from 8 repeated tests. Fig. 3 (d), (e) & (f) is the ARC test result from one cell. Cell temperature went up to 889 ºC within a few seconds. The heat generation of the cell during TR was estimated with following equations:

$$C_{total} = \frac{(C_{cell}m_{cell} + C_{can}m_{can})}{(m_{cell} + m_{can})} = 1100 \ \mathrm{Jg^{-1}K^{-1}} \quad (4)$$

Where C_{total} is the average mass specific heat of single cell, C_{cell} the average mass specific heat of the vented cell materials, C_{can} the average mass specific heat of the can and cell material residual, m_{cell} the mass of the cell materials, m_{can} the mass of the stainless steel can and m_{total} is the total mass of the single cell. According to the measurements:

$$m_{total} = m_{cell} + m_{can} = 0.047 \ \mathrm{kg} \quad (5)$$

$$Q_{total} = m_{total}C_{total}\Delta T = 0.047 \times 1100 \times (889 - 160.6) = 37658.28 \ \mathrm{J} \quad (6)$$

$$Q_{can} = m_{can}C_{can}\Delta T = 4374 \ \mathrm{J} \quad (7)$$

$$Q_{cell} = Q_{total} - Q_{can} = 33284.28 \ \mathrm{J} \quad (8)$$

$$Q_{cell}/Q_{total} = 33284.28/37658.28 = 0.88 \quad (9)$$

Where Q_{total} is the total energy released by the TR cell, Q_{can} is the energy of the can and cell material residual, and Q_{cell} is the energy carried by the vented cell materials.

2.3 Experimental study of TR propagation within a test unit

There are several methods to initiate the TR such as nail penetration, heating and overcharge. This study used electrical resistance (Joule) heating to drive the cell into TR (Fig. 4).

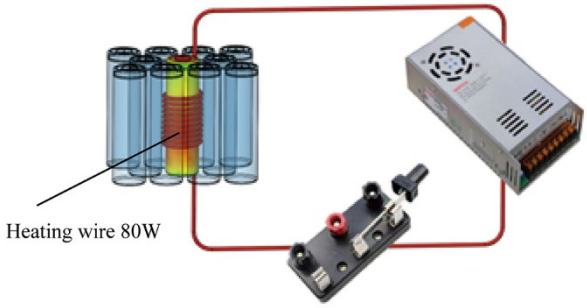

Fig. 4. Schematic of triggering process of thermal runaway by heating.

During the experiment, the triggering cell was heated to TR and forced to release energy in the form of top venting or side rupture. A gas vent is located at the top of the 18650 cell to allow for an internal pressure release when gas builds up inside the cell. Large amount of gas generated inside the cell at TR state would sharply increase internal pressure which could mostly activate the gas vent and release gas from the top of the cell. The practical application of the technique to avoid side rupture is to weaken the strength of the top or the base of cell [37]. Therefore, based on the contrary concept, the top of the cell was enhanced to increase the chance of side rupture. In this experiment, the top of the cell was glued and attached with a metal plate for reinforcement to achieve side rupture intentionally.

Commercial cells (Samsung 18650-33G) were used, which are brand new and on-purpose purchased for the experiment. The anode material of the cell is NCA (NiCoAl), the cathode material is graphite, and the electrolyte is mainly ethylene carbonate (EC) with $LiPF_6$. Cells were assembled into a BSU and the assembly procedure is illustrated in Fig. 5 (a)-(d). Cells were set between two symmetrical ABS plastic sheet, and the battery spacing were kept 2 mm. A resistance heating wire ($Cr_{20}Ni_{80}$) was wound around cell #7 in the central section of the cell (Fig. 5 (l)) for 8 rounds. The winding area accounts for half of the surface area of the cell. Cell #7 was heated during the experiment as triggering cell. The thermal couples were erected against the central surface of each cell, located on the side away from cell #7 (Fig. 5 (e), (m), Fig. 6 (c)). The signals from the thermal couples were collected by a data logger (LR8400-21, HIOKI Japan) (Fig. 7(b)), and the temperatures of the cells were recorded in real time.

Different materials were inserted in the interval between the cells, and their materials are listed in Table 2. The arrangements of interstitial layers are illustrated in Fig. 5(g)-(j). The thickness of both Al plates and graphite sheets are 2.1 mm. When BSU is assembled, the cell and the interstitial material are closely contacted (Fig. 5 (k)). BSU is locked by bolts. Tiny gaps are inevitable but can be ignored in the actual assembly. It should be noted that the graphite sheets are sandwich structures. And the outer layers are graphite (0.2 mm thickness) with the thermal conductivity of 800 W m^{-1} K^{-1} in plane direction and 25 W $m^{-1}K^{-1}$ in axial direction, while the middle layer (1.7 mm thickness) is a thermal barrier with the thermal conductivity of 0.02 W m^{-1} K^{-1}.

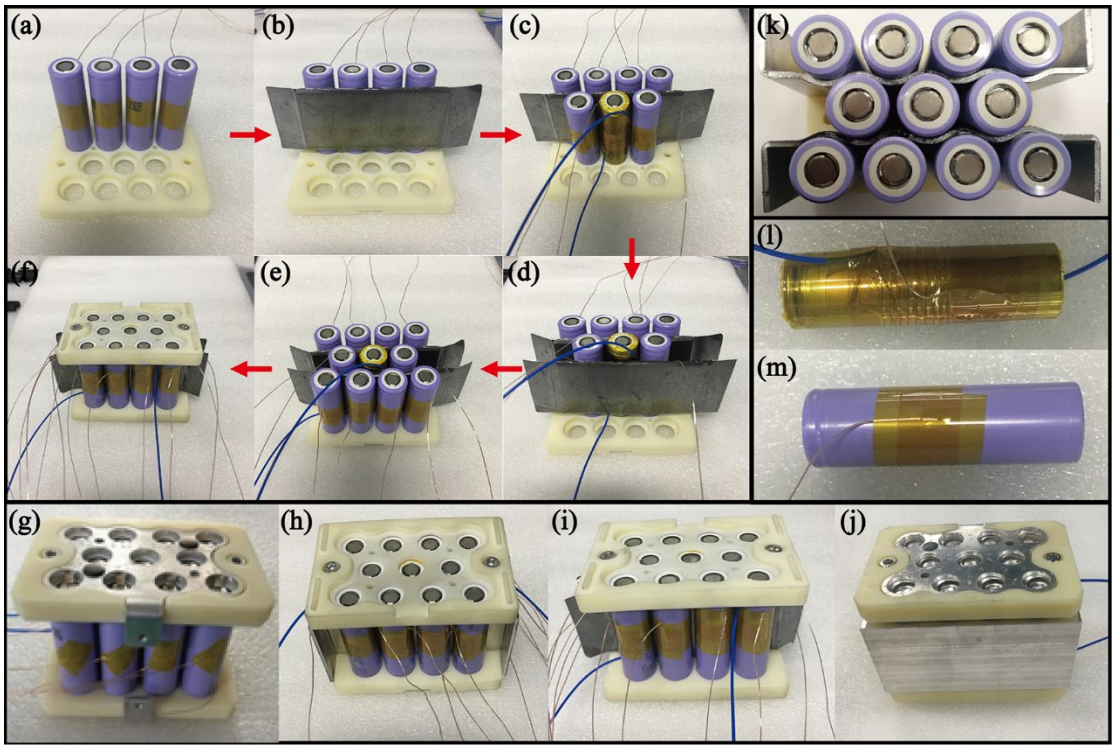

Fig. 5. Photographs of BSU modules with different interstitial material. (a)-(d) Assembling procedure for BSU (with graphite sheet); (g)-(j) BSU with different interstitial materials: (g)Air (natural state), (h) Al plate, (i) Graphite composite sheet, (j) Al extrusion; (k) top view of uncovered BSU; (l) triggering cell binding with heating wire and thermal couple in the central section of the cell; (m) neighboring cell binding with a thermal couple.

Eight BSUs were assembled with 4 interstitial materials and 2 venting options. All the BSUs were charged to 100% SOC (Fig. 6(a)) and sealed in a casing made of aluminum (Fig. 6(b)). The Al casing has a gas vent on the top. Fig. 6 shows an exploded

view, which exhibits the configurational structure. The Al casing structure was settled into a test chamber (1000 mm x 500 mm x 500 mm, 3 mm thickness, made of steel) as shown in Fig. 7(a) for experiment, which simulated the TR in a battery pack and ensured safety.

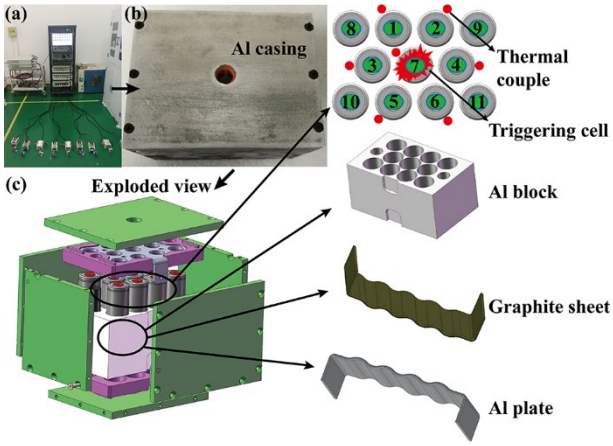

Fig. 6. Photograph and schematic of a BSU. (a) Charging setup for BSU. (b) BSU sealed in Al casing. (c) BSU configuration showing cell numbers and locations of triggered cell (cell 7) and adjacent cells (cell1-10). Thermal couples were placed on cell 1-7, while their positions are represented by red dots.

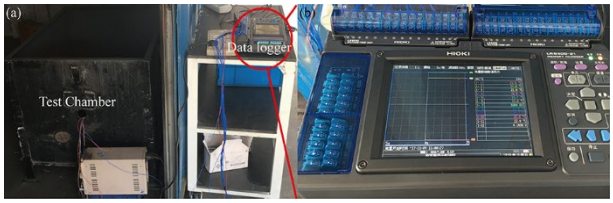

Fig. 7. Devices for thermal runaway experiment

During the experiment, the heating wire heated up cell #7 at power of 80 W by the resistance heating wire until cell #7 run into TR. The temperatures of all cells were recorded in real time.

Table 2

Characteristics of Samsung 18650-33G and different interstitial materials

Item	Density ($kg\ m^{-3}$)	Cp($J\ kg^{-1}\ K^{-1}$)	Thermal Conductivity($W\ m^{-1}\ K^{-1}$)

Samsung 18650-33G	2800	1143	Radial	Axial
			5	1
Al plate	2700	880	230	230
Graphite composite	2200	700	plane/axial	barrier
sheet (lightweight)			800/25	0.02
Al extrusion	2700	880	230	230

263

264 *2.4 Simulation process*

265 The simulation is based on the BSU containing 11 cells in parallel with various
266 interstitial materials. The center cell was triggered into energy releasing in the form of
267 top venting or side rupture. The released energy was transferred to the neighboring cells
268 through conduction, convection (natural and forced convection) and radiation.
269 Interstitial materials are directly in contact with the enclosure of BSU, which exchanges
270 heat with surroundings by convection, as shown in Fig. 6. Mesh of the model is
271 established by the meshing tool Hypermesh. Nodes between the cell and the interstitial
272 material and those between the interstitial material and the enclosure are
273 continuous/uninterrupted, as shown in Fig. 8(a).

274 Finite element method software - Fluent [38] is employed to simulate and analyze
275 the ability of various interstitial materials to restrain the temperature rise of the
276 neighboring cells, and furthermore supply theoretical guidance for the TR propagation
277 in battery module level. The maximum temperature of each single cell will be achieved
278 during the simulation process. Boundary conditions of the simulation are as follows:
279 ambient temperature is 27 ^{o}C; the Al casing is set to have a gas vent in the top to
280 simulate the real situation of the cell in a module; the gas ejected during the top venting
281 is exhausted outside the casing, while the gas ejected during the side rupture is
282 contained in the casing; the heat exchange between Al casing and external environment
283 is natural convection with gravity; the battery casing is in intimate contact with the
284 interstitial material. The middle cell of the module is set to release energy in the form
285 of top venting and side rupture as shown in Fig. 8(b). Graphite composite sheet and Al

plate are in direct contact with the surface of cell body, and the interface contact thermal resistance is ignored. In side rupture condition, hot gas energy is contained within the enclosure.

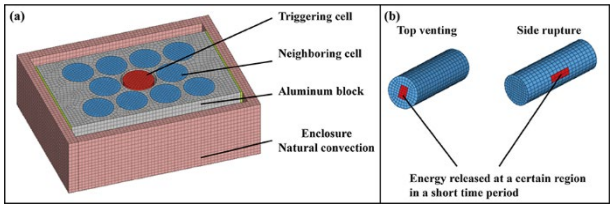

Fig. 8. Simulation model diagram. (a) Schematic of model mesh for numerical simulation; (b) Two modes of energy releasing: top venting and side rupture.

The simulation model is composed of enclosure, ABS plastic plates, thermal pad, four kinds of interstitial materials, cells with 2 mm gap, which is the same as the experiments. For comparation purpose, two mesh sizes (0.5 mm and 1 mm) are produced with 2.33 M and 0.6 M structured meshes, respectively. And nodes are continuous between meshes. No difference is observed between two results. For faster calculation convergence, 1 mm mesh size and continuous nodes between meshes is set for simulation. The ambient temperature is set at 27 ^{o}C and material properties are shown in Table 2. The quantified energy released by the triggering cell is illustrated in Fig. 3(d) & (e) and Eqs. (4)-(8). And the heat transfer coefficient of convection between the shell and the ambient surrounding is 5 W m^{-2} K^{-1}.

3. Results and discussion

The presented work details the TR propagation behavior of the BSUs with both simulation and experiment methods. The center cell was heated into TR. Meanwhile, the temperatures of the center cell and 6 abutting cells were monitored in real-time during the experiments. Experimental and simulation results with different interstitial materials are elaborated in Fig. 9 and Fig. 10, separately.

3.1 Experimental results

Eight BSUs with four different interstitial materials were tested. Cell #7 at the center was heated to TR in the mode of either top venting or side rupture, and the

temperatures of cells were recorded. Experimental results are shown in Fig. 10. The relationship between the serial number and the interstitial materials is the same as that in Table 3. Table 3 summarizes the results of each BSU, including TR_T and the time to TR of cell #7, maximum temperature and TR values of neighboring cells.

(a) BSU with none interstitial material and top venting mode:

TR was triggered in cell #7 after it was heated for 160 s and TR_T was recorded as 178 ºC approximately. Then the temperature of the adjacent cells rose from 33 ºC. The temperatures recorded exceeded the TR temperature (160.6 ºC), which means the occurrence of TR propagation. It should be noted that the temperature of adjacent cells around cell #7 fluctuated drastically, which might due to the unstable sporadic, intermittent hot vapor released by the surrounding TR cells.

The temperature recorded to reach TR of the experimental module is greater than TR_T of the ARC test on single cell. The reason is that ARC test is a slow heat-wait-search process under the assumption of uniform temperature within the cell. While in the BSU tests, the heating wire heats up the cell from outside at a much higher rate, and the nonuniformity of the temperature within the cell is significant. Therefore, the temperature at the outer shell of the cell is several degrees higher than that at inner part of the cell, which is the criterial to trigger TR. In the following cases, there are also varying degrees of temperature differences.

(b) BSU with none interstitial material and side rupture mode:

The temperature of cell #7 reached TR_T of 182 ºC after it was heated for 115 s. Almost immediately the temperature of the adjacent cells rose sharply and TR propagation occurred. The temperature dropped slowly not until after 350s.The temperature of cell #1 rose much slower than other cells. This may due to the reason that the side rupture direction of cell #7 is facing off the direction of cell #1. Therefore, cell #1 is not directly affected by the explosion, but is subjected to relatively slow heat radiation.

(c) BSU with Al plate as interstitial material and top venting mode:

The temperature of cell #7 reached TR_T of 184 ºC after it was heated for 240 s. There were small fluctuations of the adjacent cells' temperatures. The Al plate acts as

a heat sink and absorbs the heat energy of cell #7. The maximum temperature of the adjacent cells reached is about 120 ^{o}C, and no TR propagation occurs.

(d) BSU with Al plate as interstitial material and side rupture mode:

Cell #7 was forced to TR after heated for 240 s. The temperatures of adjacent cells rose sharply along with the TR of cell #7, and TR propagation occurred in the BSU. The energy released by side rupture of cell #7 is all wrapped in the module. The Al plate is saturated as heat sink. Therefore, the heat energy is transferred to the surrounding cells. In the case of top venting (c), part of the energy was released outside the module along with the material explosion, so no TR propagation was observed in Fig. 17(c). The direction of side rupture might face to cell #2, #4, and #6, so the temperature of these cells rose faster than cell #1, #3, and #5 as shown in the inset of Fig. 17(d). Moreover, due to the heat sink and space isolation effect of the aluminum plate, the energy dissipation is relatively stable during the cooling process of the entire module, so the temperature drop is relatively stable compared to (a) and (b).

(e) BSU with graphite composite sheets as interstitial material and top venting mode:

Cell #7 was heated to trigger TR. Moderate temperature rise (slightly above 100 ^{o}C) of the adjacent cells was recorded and no TR propagation was observed, as in the case of (c). Furthermore, the maximum temperature of the triggered cell reached about 800 ^{o}C, and is much smaller than those in modules with TR propagations, which is above 1000 ^{o}C. This is due to the large amount of energy released during TR propagations in the modules causing excessive temperature rise in the center of the modules.

(f) BSU with graphite composite sheets as interstitial material and side rupture mode:

The temperature of the center cell reached TR_T of 178 ^{o}C after it was heated for 150 s. Moderate temperature rise of the adjacent cell that is directly in the rupture direction of the TR cell was recorded. And no TR propagation was observed after temperature rise fluctuations. Hence, graphite composite sheet can prevent TR propagation in BSU even in the side rupture mode. The graphite sheet has a high

thermal conductivity in plane direction (800 W $m^{-1}K^{-1}$), which can spread out the heat released from the TR cell rapidly to the Al casing. On the other hand, the graphite sheet has a low thermal conductivity in the axial direction (25 W $m^{-1}K^{-1}$) due to the sandwich structure, which can effectively shelter the cells adjacent to the TR cell. Therefore, the temperature distribution among the whole module is quite uniform even in this side rupture mode.

(g) BSU with Al extrusion as interstitial material and top venting mode:

Cell #7 was forced to TR. TR lasted for around 10 s and the maximum temperature reached 850 ^{o}C. The temperature of the neighboring cell 3 reached highest value of 102 ^{o}C, which did not trigger TR and the rest cells remained stable.

(h) BSU with Al extrusion as interstitial material and side rupture mode:

Cell #7 was forced to TR. The temperature of adjacent cell #2 reached a maximum temperature around 115 ^{o}C, and did not trigger TR.

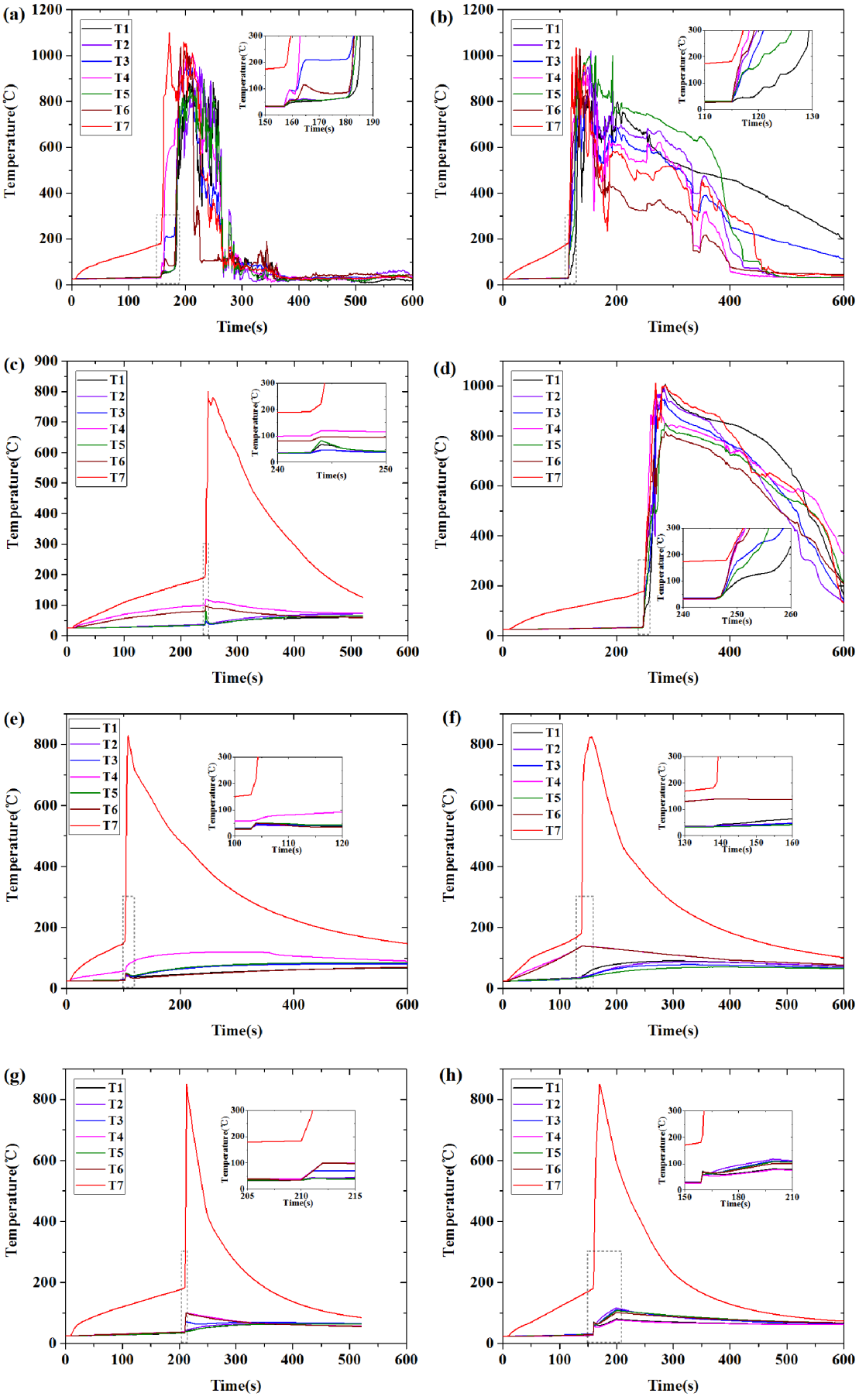
(a)
(b)
(c)
(d)
(e)
(f)
(g)
(h)
T1
T2
T3
T4
T5
T6
T7
Temperature(℃)
Time(s)

Fig. 9. Experiment results of 7 cells (a) with air as interstitial material and top venting; (b) with air as interstitial material and side rupture; (c) with Al plate as interstitial material and top venting; (d) with Al plate as interstitial material and side rupture; (e) with graphite sheet as interstitial material and top venting; (f) with graphite sheet as interstitial material and side rupture; (g) with Al extrusion as interstitial material and top venting; (h) with Al extrusion as interstitial material and side rupture.

Table 3

Summary of experiment results of all BSUs. The results include venting mode, triggering temperature and time to TR of cell #7, maximum temperatures and TR values of neighboring cells. 'T' means 'Top venting', 'S' means 'Side rupture'. 'Fail' means that TR propagation occurs in the module, while 'Pass' means that no TR propagation occurs in the module

	(a)	(b)	(c)	(d)	(e)	(f)	(g)	(h)
Interstitial material	Air(air)		Al plate		graphite composite sheet		Al extrusion	
Venting mode	T	S	T	S	T	S	T	S
Time to TR (s)	160	115	240	240	248	150	210	159
TR_T (°C)	178	182	184	180	157	178	184	181
Max Temp (°C)			120		100	120	102	115
TR value	Fail	Fail	Pass	Fail	Pass	Pass	Pass	Pass

3.2 Simulation results

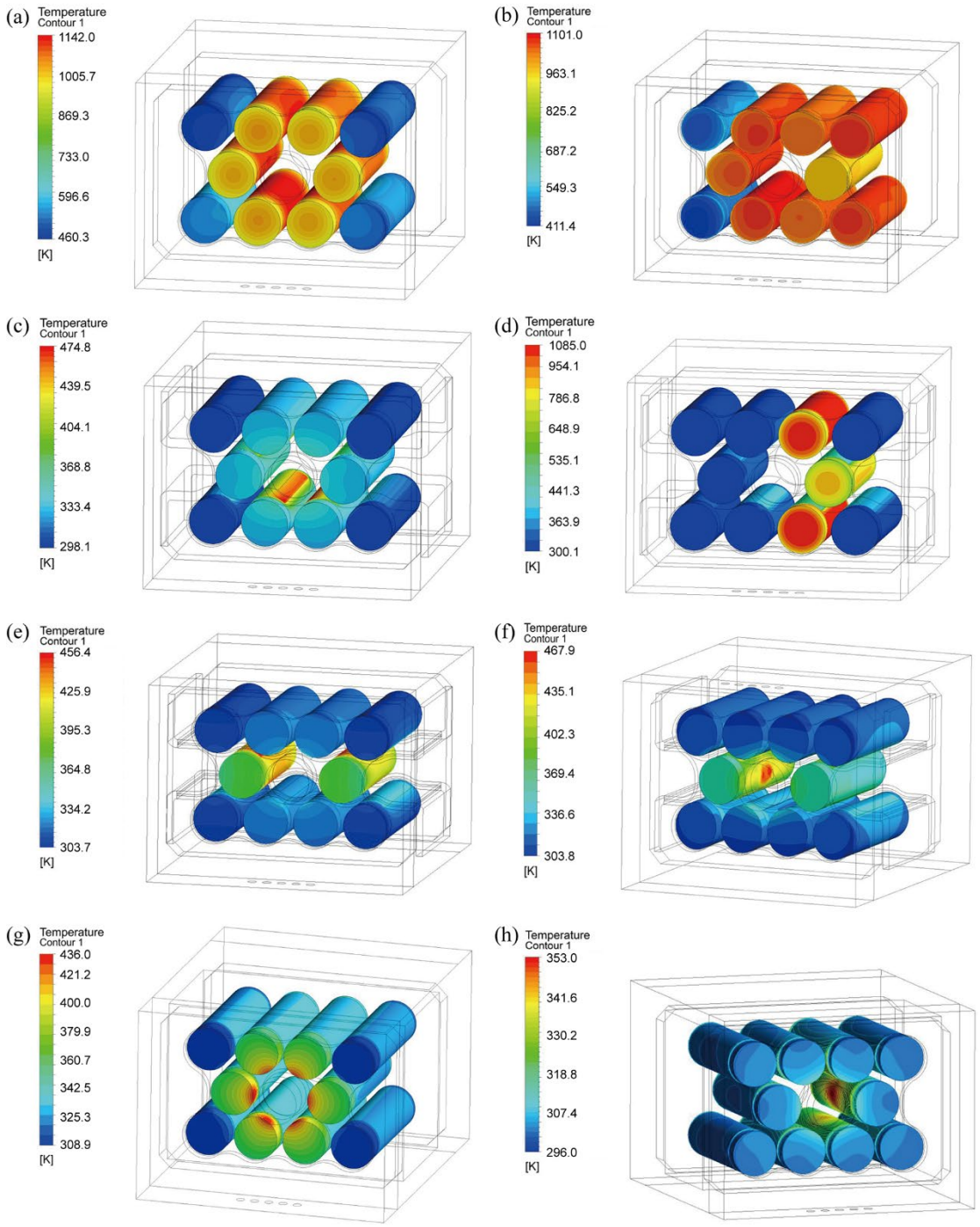

Fig. 10. Simulation results of the temperature responses of BSU (a) with air as interstitial material and top venting; (b) with air as interstitial material and side rupture; (c) with Al plate as interstitial material and top venting; (d) with Al plate as interstitial material and side rupture; (e) with graphite sheet as interstitial material and top venting; (f) with graphite sheet as interstitial material and side rupture; (g) with Al extrusion as interstitial material and top venting; (h) with Al extrusion as interstitial material and side rupture.

Fig. 10 illustrates the numerical simulation results of the temperature distribution

inside the modules with various interstitial materials. The center cell was hidden to strengthen the color difference generated from the temperature gradient since the temperature difference between neighboring cells and the center cell are drastic during the energy release process. The energy generated by chain reactions is ignored in order to reduce the complexity of simulation. It is a low cost method to evaluate the safety and reliability of module design to obtain a simple and clear criterion of thermal runaway onset. During the simulation, the energy is loaded on the center cell, whose value is determined from the ARC test. The temperature of the center cell increased to about 800 ^{o}C within 5 s after it was triggered. The neighboring cells reach their peak temperature after the center cell does. In the experiment process, the thermal couple of cell #1-#6 was erected against the central surface of each cell, located on the side facing off from cell #7 (Fig. 6 (c)). In the simulation, the temperatures of neighboring cells are monitored at locations that are facing away from the center cell, which are the same as those in the experiment. These recorded temperatures are taken as the criteria of thermal runaway onset. Sample illustration of simulated temperature results for neighboring cells is shown in Fig. 11. Temperatures rise rapidly for cells with none interstitial material and top venting mode (Fig. 11(a)), and no high temperature is found for cells with Al extrusion and side rupture mode (Fig. 11(b)). The temperatures and outcomes are shown in Table 4. The triggering temperature is 160.6±1.2 ^{o}C acquired from ARC test.

Table 4

Max temperature of neighboring cells in simulation. 'T' means 'Top venting', 'S' means 'Side rupture'. 'Fail' means that TR propagation occurs in the module, while 'Pass' means that no TR propagation occurs in the module

No.	(a)	(b)	(c)	(d)	(e)	(f)	(g)	(h)
Interstitial material	None(air)		Al plate		graphite composite sheet		Al extrusion	
Venting mode	T	S	T	S	T	S	T	S
Cell Temp.(℃)	869	828	80	812	153	120	83	80

TR value	Fail	Fail	Pass	Fail	Pass	Pass	Pass	Pass

3.3 Summary

Table 5

Results of TR experiment. 'Pass' means no TR propagation occurring in the BSU, while 'Fail' means TR propagation occurring in the BSU.

Interstitial material	Mode	Simulation results	Experiment results
Air	Top venting	Fail	Fail
	Side rupture	Fail	Fail
Al plate	Top venting	Pass	Pass
	Side rupture	Fail	Fail
Graphite composite sheet	Top venting	Pass	Pass
	Side rupture	Pass	Pass
Al extrusion	Top venting	Pass	Pass
	Side rupture	Pass	Pass

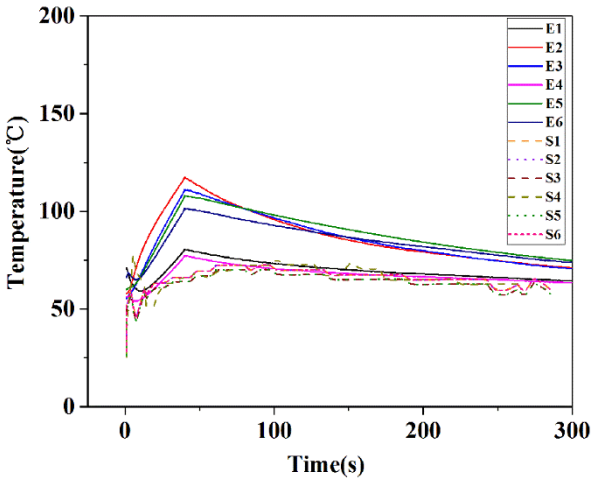

Fig. 11. Temperature results of BSU with Al extrusion as interstitial material and side rupture mode for both simulation and experiment. Curves “E1-E6” are temperature records of cell #1-#6 in experiment; Curves “S1-S6” are simulation calculated temperature results for cell#1- #6.

Temperature results of BSU with Al extrusion as interstitial material and side

443 rupture mode for both simulation and experiment are shown in Fig. 11. The
444 temperatures of neighboring cells #1-#6 agreed well, which provides a basis for
445 consistency of simulation and experimental results.

446 The simulation and experiment results are summarized in Table 5. The outcomes
447 of the experiments are shown in Fig. 12. Generally, the results of experiment and
448 simulation agreed well, except certain temperature differences. From the simulation and
449 experimental results, it can be seen that under the current module energy density and
450 battery spacing conditions, only air in the gap cannot prevent the TR propagation in any
451 form. In the case of top venting, the aluminum plate has the function of heat sink and
452 heat conductor, which successfully prevents the TR propagation, but is overwhelmed
453 in the case of side rupture. The graphite composite plate and Al extrusion can
454 successfully prevent the TR propagation under both modes (top venting and side
455 rupture). The high in-plane thermal conductivity of the graphite in the graphite
456 composite plate and the thermal insulation of the intermediate interlayer effectively
457 prevent the heat from being transferred to adjacent cells. The Al extrusion can absorb
458 the heat generated from the TR cell as a robust heat sink, which can effectively prevent
459 the TR propagation.

460

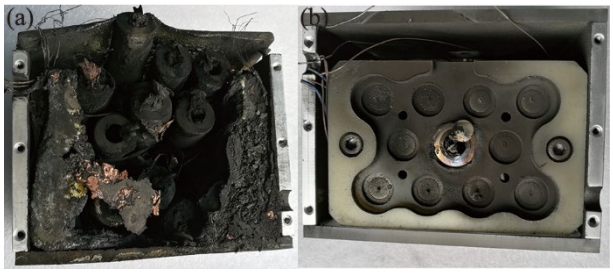

461

462 **Fig. 12.** BSUs with (a) and without (b) the propagation of thermal runaway.

463 Graphite composite plates are light in weight but expensive, and are not suitable
464 for common consumer product applications. It is suitable for applications where energy
465 density and safety requirements are relatively high, such as space and military battery
466 unit. The Al extrusion is relatively heavy but has a lower cost than graphite composite
467 sheet, and it can prevent the TR propagation mostly. It can be used in the case of weight-
468 insensitive products such as heavy duty electric machines, energy storage power

469 stations.

470

471 **4. Conclusion**

472 The objective of this study is the inhibition effect on TR propagation utilizing
473 different interstitial materials when TR of a cell occurs in a module. Four interstitial
474 materials were evaluated in both simulation and experimental methods. And the
475 commercial application prospects of the battery module design were also discussed. In
476 this study, modules composed of 11 cells with four interstitial materials (air, Al plate,
477 graphite composite sheet and Al extrusion) were built as the basic test units. The TR
478 conditions and properties of a single cell were calibrated by ARC test. In simulation
479 these properties were loaded on the center cell as initial condition to calculate the
480 temperature distribution of the neighboring cells, while the chain reactions were not
481 considered. The center cell was triggered into TR by an 80W heating wire and the
482 temperature of all the cells were monitored in the experiment process.

483 TR is a drastic energy releasing process, especially in side rupture condition. In
484 battery module design, air alone cannot prevent the TR propagation. Aluminum plate
485 has a certain safety protection against TR，but failed in the case of side rupture. The
486 graphite composite sheet can significantly prevent the TR propagation, due to the high
487 in-plane thermal conductivity of the graphite sheet layers and relatively low thermal
488 conductivity in cross-plane direction of the graphite sheet layers, particularly the high
489 thermal insulation and fire resistance of intermediate layer. Even though Al extrusion
490 is slightly heavy, but it shows the best performance in restraining TR propagation,
491 which can stabilize the temperature of the entire module in a moderate range. This
492 approach is most likely to be applicable for lithium-ion batteries which have an energy
493 density not higher than that used. At present, the results of this study are more inclined
494 to be applied to cylindrical batteries. It may also be useful for prismatic and pouch cells
495 with higher energy, while the structure design and material parameters need to be
496 further adjusted according to different application states.

497 It can be seen that side rupture of the triggering cell can significantly increase the

possibility of TR propagation and managing the top venting path is critical for thermal management. It is a feasible way to improve the safety of the high specific energy lithium ion battery by utilizing different interstitial materials to change the thermal path in the battery module. A proper safety valve should be designed in the bottom of cell to release the pressure and heat, which is a critical means to help avoiding side rupture. Furthermore, for safety concern, the combustion of expelled electrolyte must be directed away from adjacent cells in the battery packs.

Acknowledgments

This work was supported by the National Natural Science Foundation of China (#11572311 and #11772321) and the Chinese 1000 Young Talented Program. The authors wish to thank USTC Center of Micro and Nanoscale Research and Fabrication for providing the experimental facilities used in this work.

References

[1] X. Shan, F. Li, D. Wang, H. Cheng, The smart era of electrochemical energy storage devices, Energy Storage Mater. 3 (2016) 66-68.

[2] J.B. Dunn, L. Gaines, J.C. Kelly, C. James, K.G. Gallagher, The significance of Li ion batteries in electric vehicle life-cycle energy and emissions and recycling's role in its reduction, Energy Environ. Sci. 8 (2015) 158-168.

[3] D. Liu, H. Wang, Y. Peng, W. Xie, H. Liao, Satellite lithium-ion battery remaining cycle life prediction with novel indirect health indicator extraction, Energies 6 (2013) 3654-3668.

[4] E. Darcy, Thermal runaway Severity Reduction Assessment for EVA Li-ion Batteries, Huntsville, Alabama, 2014.

[5] W. Walker, S. Yayathi, J. Shaw, H. Ardebili, Thermo-electrochemical evaluation of lithium-ion batteries for space applications, J. Power Sources 298 (2015) 217-227.

[6] Y. Xie, J. Tang, S. Shi, Y. Xing, H. Wu, Z. Hu, Experimental and numerical investigation on integrated thermal management for lithium-ion battery pack with composite phase change

526 materials, Energy Convers. Manage. 154 (2017) 562-575.
527 [7] C. Lopez, J. Jeevarajan, P. Mukherjee, Experimental analysis of thermal runaway and
528 propagation in lithium-ion battery modules, J. Electrochem. Soc. 162 (2015) 1905-1915.
529 [8] A.W. Golubkov, D. Fuchs, J. Wagner, H. Wiltsche, C. Stangl, G. Fauler, et al., Thermal-
530 runaway experiments on consumer Li-ion batteries with metal-oxide and olivin-type cathodes,
531 RSC Adv. 4 (2014) 3633-3642.
532 [9] X. Feng, X. He, M. Ouyang, L. Lu, P. Wu, C. Kulp, et al., Thermal runaway propagation model
533 for designing a safer battery pack with 25Ah LiNix-CoyMnzO2 large format lithium ion
534 battery, Appl. Energy 154 (2015) 74-91.
535 [10] W. Wu, X. Yang, G. Zhang, K. Chen, S. Wang, Experimental investigation on the thermal
536 performance of heat pipe-assisted phase change material based battery thermal management
537 system, Energy Convers. Manage. 138 (2017) 486-492.
538 [11] A. Melcher, C. Ziebert, M. Rohde, B. Lei, H.J. Seifert, Modeling and Simulation of the
539 Thermal Runaway Behavior of Cylindrical Li-Ion Cells - Computing of Critical Parameters,
540 Energies 9 (2016) 292.
541 [12] D.P. Abraham, E.P. Roth, R. Kostecki, K. McCarthy, S. MacLaren, D.H. Doughty, Diagnostic
542 examination of thermally abused high-power Lithium-ion cells, J. Power Sources 161 (2006)
543 648-657.
544 [13] D. Hyup Jeon, S. Man Baek, Thermal modeling of cylindrical lithium ion battery during
545 discharge cycle, Energy Convers. Manage. 52 (2011) 2973-2981.
546 [14] A. Mills, M. Farid, J.R. Selman, S. Al-Hallaj, Thermal conductivity enhancement of phase
547 change materials using a graphite matrix, Appl. Therm. Eng. 26 (2006) 1652-1661.
548 [15] Q. Wang, P. Ping, X. Zhao, G. Chu, J. Sun, C. Chen, Thermal runaway caused fire and
549 explosion of lithium ion battery, J. Power Sources 208 (2012) 210-224.
550 [16] R. Walters, R.E. Lyon, Energy release from lithium ion batteries in the bomb calorimeter, in:
551 Proceedings of the Fire and Materials Conference, San Fran-cisco, 2015 78-86.
552 [17] X. Xu, R. He, Review on the heat dissipation performance of battery pack with different
553 structures and operation conditions, Renew. Sustain. Energy Rev. 29 (2014) 301-315.
554 [18] Z. Rao, S. Wang, A review of power battery thermal energy management, Renew. Sustain.
555 Energy Rev. 15 (2011) 4554-4571.

556 [19] J. Xun, R. Liu, K. Jiao, Numerical and analytical modeling of lithium ion battery thermal
557 behaviors with different cooling designs, J. Power Sources 233 (2013) 47-61.
558 [20] J. Wen, Y. Yu, C. Chen, A review on lithium-ion batteries safety issues: existing problems and
559 possible solutions, Mater. Express 2 (2012) 197-212.
560 [21] X. Feng, M. Ouyang, X. Liu, L. Lu, Y. Xia, X. He, Thermal runaway mechanism of lithium
561 ion battery for electric vehicles: A review, Energy Storage Mater. 10 (2018) 246-267.
562 [22] H. Fathabadi, High thermal performance lithium-ion battery pack including hybrid active-
563 passive thermal management system for using in hybrid/electric vehicles, Energy, 70 (2014)
564 529-538.
565 [23] J. Zhao, Z. Rao, Y. Huo, X. Liu, Y. Li, Thermal management of cylindrical power battery
566 module for extending the life of new energy electric vehicles, Appl. Therm. Eng. 85 (2015)
567 33-43.
568 [24] L. H. Saw, Y. Ye, A. A. O. Tay, Feasibility study of Boron Nitride coating on Lithium-ion
569 battery casing, Appl. Therm. Eng. 73 (2014) 154-161.
570 [25] P. T. Coman, S. Rayman, R. E. White, A lumped model of venting during thermal runaway in
571 a cylindrical Lithium Cobalt Oxide lithium-ion cell, J. Power Sources 307 (2016) 56-62.
572 [26] G. Guo, B. Long, B. Cheng, S. Zhou, P. Xu, B. Cao, Three-dimensional thermal finite element
573 modeling of lithium-ion battery in thermal abuse application, J. Power Sources 195 (2010)
574 2393-2398.
575 [27] B. Liu, Three dimensional thermal modeling of lithium-ion battery pack for electric vehicles
576 thermal management, M.Sc. thesis, Hong Kong University of Science and Technology, 2014.
577 [28] L. H. Saw, Y. Ye, M. C. Yew, W. T. Chong, M. K. Yew, T. C. Ng, Computational fluid
578 dynamics simulation on open cell aluminium foams for Li-ion battery cooling system, Appl.
579 Energy 204 (2017) 1489-1499.
580 [29] D. Ouyang, J. Liu, M Chen, J Weng and J. Wang, Thermal Failure Propagation in Lithium-Ion
581 Battery Modules with Various Shapes, Appl. Sci. 8 (2018) 1263.
582 [30] J. Lamb, C. J. Orendorff, L. A. M. Steele, S. W. Spangler, Failure propagation in multi-cell
583 lithium ion batteries, J. Power Sources 283 (2015) 517-523.
584 [31] S. Abada, G. Marlair, A. Lecocq, M. Petit, V. Sauvant-Moynot, F. Huet, Safety focused
585 modeling of lithium-ion batteries: A review, J. Power Sources 306 (2016) 178-192.

586 [32] W. Chen, Y. Wang, C. Shu, Adiabatic calorimetry test of the reaction kinetics and self-heating
587 model for 18650 Li-ion cells in various states of charge, J. Power Sources 318 (2016) 200-209.
588 [33] T. D. Hatchard, D. D. MacNeil, A. Basuc and J. R. Dahn, Thermal Model of Cylindrical and
589 Prismatic Lithium-Ion Cells, J. Electrochem. Soc. 148 (2001) 755.
590 [34] G. Kim, A. Pesaran, R. Spotnitz, A three-dimensional thermal abuse model for lithium-ion
591 cells, J. Power Sources 170 (2007), 476.
592 [35] P. Wu, J. Romberg, X. Feng, M. Zhang, L. Lu, X. He, M. Ouyang, Thermal Runaway
593 Propagation Within Module Consists of Large Format Li-Ion Cells. Proceedings of SAE-China
594 Congress 2015: Electrical Engineering 364.
595 [36] A. W. Golubkov, D. Fuchs, J. Wagner, H. Wiltsche, C. Stangl, G. Fauler, G. Voitic, A. Thaler,
596 V. Hacker. Thermal-runaway experiments on consumer Li-ion batteries with metal-oxide and
597 olivin-type cathodes. RSC Advances 4(2014) 3633.
598 [37] D. P. Finegan, Identifying the Cause of Rupture of Li‐Ion Batteries during Thermal Runaway,
599 Adv. Sci. 5 (2018) 170-369.
600 [38] Fluent User's Guide: Version 14.0, 2014.